12th AIAA Aviation Technology, Integration, and Operations (ATIO) Conference and 14th AIAA/ISSM
17 - 19 September 2012, Indianapolis, Indiana

AIAA 2012-5656

An Adjoint-Based Multidisciplinary Optimization Framework for Rotorcraft Systems

M. R. Colonno[1], K. Naik[2], K. Duraisamy[3], and J. J. Alonso[4]
Stanford University, Dept. of Aeronautics & Astronautics, Stanford, CA, 94305

A new architecture for multidisciplinary optimization of rotorcraft systems is presented and compared to those previously used. This architecture rearranges the inner loop (soft coupling between a high-fidelity aerodynamics and comprehensive structural dynamics), moving the expensive computational fluids analysis out. Continuous adjoint surface sensitivities and free-form geometric deformation are used for aerodynamic shape optimization with the corresponding surface sensitivities used to approximate small changes in the aerodynamic loading on the blade in a modified coupling procedure. The resulting framework allows for a lower-cost optimization process to be performed using only the comprehensive rotorcraft code with a large number of design variables. Preliminary results are presented for a single-blade model and future research directions are discussed.

Nomenclature

a	=	speed of sound
c	=	airfoil chord length
$\vec{d}$	=	force projection vector
j_S	=	scalar function defined on surface S
$\vec{n}$	=	unit normal vector
p	=	static pressure
t_0	=	initial time
t_f	=	final time
$\vec{u}_b$	=	control volume boundary velocity
$\vec{v}$	=	flow velocity vector in inertial frame
V_∞	=	free stream velocity
$\vec{A}$	=	inviscid flux Jacobian matrices
E	=	total energy per unit mass
H	=	stagnation enthalpy
A_D	=	rotor disk area (πR^2)
C_P	=	power coefficient ($Q\omega/\rho_\infty V_T^2 A_\mathrm{D}$)
c_l	=	airfoil lift coefficient ($l/q_\infty c$)
c_d	=	airfoil drag coefficient ($d/q_\infty c$)
C_T	=	thrust coefficient ($F_\mathrm{T}/q_\infty A_\mathrm{D}$)
C_Q	=	torque coefficient ($Q/q_\infty A_\mathrm{D} R$)
R	=	rotor radius
F_T	=	thrust force
D	=	drag force
M	=	Mach number
d	=	drag force per unit length
L	=	lift force

[1] Engineering Research Associate, Department of Aeronautics & Astronautics, Stanford University.
[2] Ph.D. Candidate, Department of Aeronautics & Astronautics, Stanford University.
[3] Consulting Professor, Department of Aeronautics & Astronautics, Stanford University.
[4] Associate Professor, Department of Aeronautics & Astronautics, Stanford University.

l = lift force per unit length
Q = rotor torque
V_T = blade tip speed
x,y,z = blade-fixed coordinates
J = objective function
$R(U)$ = system of governing flow equations
S = solid wall boundary (design surface)
U = vector of conservative variables
$\mathbf{x}$ = vector of design variables
α = angle of attack
β = side-slip angle
ρ = density
ρ_∞ = free-stream density
$\vec{\varphi}$ = flow adjoint velocity vector
Γ = domain boundary
ψ = vector of flow adjoint variables
Ω = problem domain
γ = ratio of specific heats
ω = rotation frequency
ϕ = rotation angle (azimuth)
$\nabla(\cdot)$ = gradient operator
$\nabla\cdot(\cdot)$ = divergence operator
$\partial_n(\cdot)$ = surface-normal gradient operator, $\vec{n}_S \cdot \nabla(\cdot)$
$\cdot$ = vector inner product
x = vector cross product
$\otimes$ = vector outer product
$\delta(\cdot)$ = first variation

I. Introduction

IN in this study we develop a multidisciplinary framework for the optimization of rotorcraft systems using coupled, high-fidelity analysis tools, variable computational cost, and standard optimization techniques. Previous study by Choi, Datta, Potsdam, Alonso, and others[3-9,14,15,22] , have demonstrated the capability of design tools based on time-accurate or time-spectral flow solutions, adjoint-based sensitivities, comprehensive rotorcraft tools (handling structural dynamics and possibly vehicle trim), and widely-accepted shape optimization techniques applied to the problem of a helicopter rotor blade in unsteady, periodic, forward flight or hover. These studies included aeroelastic coupling (using varying methods) and varying approximations of trim conditions. Earlier work involved only hover conditions (which can be studied with far less expensive steady flow solutions) for which only airfoil shape changes were considered in optimization. As three-dimensional flow solution tools and computational power improved, high-fidelity hover and forward flight cases could be considered for optimization. Forward flight optimization of a three-dimensional rotor blade using high fidelity computational fluid dynamic (CFD) methods, however, has only recently been enabled with advances in the time-spectral and time-accurate CFD methodology. Many previous rotor optimization methods utilized low fidelity aerodynamics (such as lifting line and vortex wakes) embedded in rotorcraft comprehensive codes[25] in order to handle the multidisciplinary nature of the problem.

The present work extends the previous research in three general areas:

(1) Trim conditions were treated as a serial processing step in the global optimization process to ensure trim at each major iteration (and hence at convergence).
(2) A more generalized parameterization of the three-dimensional blade geometry using free-form deformation boxes.
(3) The use of adjoint-based aerodynamic surface sensitivities to reduce the computational cost and coupling requirements.

The design and optimization environment is based on the Stanford University Unstructured (SU^2)[20,24] design environment which enables both flow solutions and a continuous adjoint formulation. The adjoint solution capability yields the sensitivity of the quantity of interest to surface-normal displacement of any node. This capability is extended via the use of free-form-deformation (FFD) boxes which allow for generalized modification of geometry while dramatically reducing the number of design variables (when compared to the number of surface nodes). Combined, these capabilities enable accurate gradients for design, an arbitrary level of detail in geometry perturbation, and an arbitrarily-sized design space. Rotorcraft applications (with the exception of hover) require either a time-accurate or time-spectral treatment. Here, a time-accurate simulation was used with the quantities of interest, C_Q and C_T, and the corresponding adjoint solutions, averaged over a revolution of the rotor.

These results were coupled with a comprehensive rotorcraft or comprehensive structural dynamics (CSD) tool, the University of Maryland Advanced Rotorcraft Code (UMARC)[26]. UMARC solves the coupled structural dynamic and control problem to yield a trimmed vehicle (including rotor and body). Its structural simulation capabilities are based upon Euler-Bernoulli beam theory and hence treats a given rotor blade as a one-dimensional structure consisting of airfoil sections. It therefore depends upon an external aerodynamic analysis (and or a lower-fidelity aerodynamic simulation) to provide the performance of each airfoil section along the radius of the blade at each azimuth. Hence, CSD tools are often "soft-coupled" with CFD tools to provide a high-fidelity replacement for the lower-fidelity aerodynamic models incorporated into UMARC and other CSDs. "Soft" coupling involves iteratively using each tool, providing the required inputs from one to the other. This is contrasted with "hard" or "tight" coupling in which the two tools are used simultaneously in a time-accurate or time-spectral fashion. In this case, CSD provides the translational and rotational deflections to the CFD analysis (which must include mesh motion capabilities) while CFD provides the aerodynamic loads at each airfoil section. Typically, this coupled process is iterated to convergence for each design considered in an optimization process.

In this study, the traditional soft-coupled approach was modified to take advantage of the availability of adjoint surface sensitivities and reduce the computational load of the optimization process. The CFD portion of the process described above comprises the vast majority of the total computational cost. This is exacerbated by the complexity of the CFD analysis itself: three-dimensional, time accurate (or time spectral), transonic (near the blade tips), and including mesh deformation on a significant scale relative to the geometry. Together, these typically require conservative settings be used to ensure convergence of any possible design in the design space. Reducing the number of CFD evaluations required to optimize a rotor system is key to enabling more detailed designs. By using a flow solution, and adjoint solution of the torque coefficient (C_Q), and an adjoint solution of the thrust coefficient (C_T), approximately three CFD solutions are required to provide not just the solution data itself (specifically the airfoil section loads) but also a linear approximation to aerodynamic performance due to perturbations in the blade geometry. Hence, the CSD tool (inexpensive by comparison) and the linearized aerodynamic model can used together to produce a first optimum design via sequential linear programming (SLP). The flow and adjoint solutions can then be run again, asynchronously to the optimization procedure, to produce a new linearized model. This procedure can then repeated to the desired level of convergence with considerably fewer total CFD evaluations.

In the subsequent sections we present the process discussed above in detail in addition to preliminary results of its application to a UH-60A rotor blade under high-speed, forward flight conditions. A single blade was modeled in inviscid flow in order to minimize computational cost, though the method is unchanged for a full rotor in viscous flow. A free-form deformation box around the outer half of the blade was used to perturb the geometry and a standard sequential quadratic programming algorithm was used for optimization. The minimization of torque was used as the objective with a minimum thrust constraint. The optimum design from the linearized aerodynamic model was then trimmed in UMARC with updated aerodynamic loading and geometry. The following sections detail the methodology used, the high-fidelity aerodynamic and adjoint analyses, the optimization procedure, the resulting (initial) optimum design, and the many improvements to the methodology and future directions to be taken.

This paper is organized as follows. In the following section the continuous adjoint method for computing surface sensitivities to aerodynamic performance is discussed. This is then extended to yield an approximation for local two-dimensional airfoil aerodynamic properties along the blade. Next, the global MDAO architecture is discussed and contrasted to previous methods used for rotorcraft optimization based on soft coupling of each design iteration. Finally, preliminary results of initial tests of the method are presented and future research directions are discussed.

II. Governing Flow and Adjoint Problems for Unsteady Aerodynamics

This section contains a summary of the governing flow equations and corresponding time-accurate continuous adjoint formulation for the aerodynamic analysis and design portion of this MDAO problem.

A. Description of the Physical Problem

Ideal fluids are governed by the Euler equations. In our particular problem, these equations are considered in a domain, Ω, bounded by a disconnected boundary which is divided into a far-field component, Γ_∞, and a solid wall boundary, S, as seen in Fig. 1. The surface S will also be referred to as the design surface and it is considered continuously differentiable (C^1). Normal vectors to the boundary surfaces are directed out of the domain by convention.

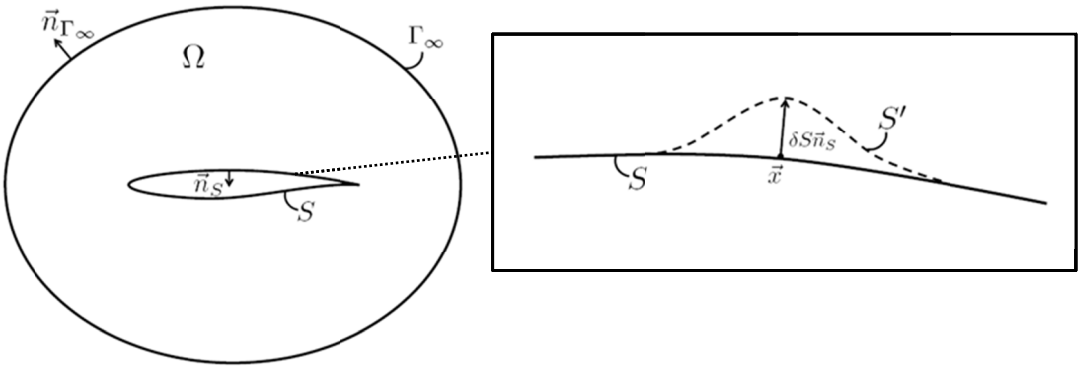

Figure 1. Schematic of volume and surface domains for the continuous adjoint formulation with surface shape perturbation.

We are interested in time-accurate fluid behavior around aerodynamic bodies in arbitrary motion for situations where viscous effects can be considered negligible. The governing flow equations in the limit of vanishing viscosity are the compressible Euler equations which can be expressed in conservation form as

$$\begin{aligned} &\frac{\partial U}{\partial t} + \nabla \cdot \vec{F}_{mov} = 0 && \text{in } \Omega \\ &\left(\vec{v} - \vec{u}_b\right) \cdot \vec{n}_S = 0 && \text{on } S \\ &W^+_{\Gamma_\infty}(U) = W_\infty && \text{on } \Gamma_\infty, \end{aligned} \tag{1}$$

where

$$U = \begin{Bmatrix} \rho \\ \rho\vec{v} \\ \rho E \end{Bmatrix}, \vec{F}_{mov} = \begin{Bmatrix} \rho(\vec{v} - \vec{u}_b) \\ \rho\vec{v} \otimes (\vec{v} - \vec{u}_b) + \bar{\bar{I}}p \\ \rho E(\vec{v} - \vec{u}_b) + p\vec{v} \end{Bmatrix}, \tag{2}$$

ρ is the fluid density, $\vec{v} = \{u, v, w\}^T$ is the flow velocity, $\vec{u}_b$ is the boundary velocity for a control volume in motion, E is the total energy per unit mass, and p is the static pressure. The second line of Eqns. (1) represents the flow tangency condition at a solid wall. The final line represents a characteristic-based boundary condition at the far-field where, in general, the fluid states at the boundaries are updated depending on the sign of the eigenvalues. The boundary conditions take into account any boundary velocity due to control volume motion. In order to close the system of equations after assuming a perfect gas, the pressure is determined from

$$p = (\gamma - 1)\rho\left[E - \frac{1}{2}(\vec{v} \cdot \vec{v})\right], \tag{3}$$

and the stagnation enthalpy is given by

$$H = E + \frac{p}{\rho}. \tag{4}$$

B. Surface Sensitivities via a Time-Accurate Continuous Adjoint Approach

The objective of this section is to describe the way in which we quantify the influence of geometric modifications on the pressure distribution at a solid surface in the flow domain.

A typical shape optimization problem seeks the minimization of a certain cost function, J, with respect to changes in the shape of the boundary, S. Therefore, we will concentrate on functionals defined as time-averaged integrated quantities on the solid surface S,

$$J = \frac{1}{T}\int_{t_o}^{t_f}\int_{S} j_S \, ds dt, \tag{5}$$

where j_S is a time-dependent scalar function defined at each point on S.

Therefore, the goal is to compute the variation, or change, of Eqn. (5) caused by arbitrary but small (and multiple) deformations of S and to use this information to drive our geometric changes in order to find an optimal shape for the design surface, S. This leads directly to a gradient-based optimization framework. The shape deformations applied to S will be infinitesimal in nature and can be described mathematically by

$$S' = \left\{ \vec{x} + \delta S(\vec{x}) n_S(\vec{x}), \vec{x} \in S \right\}, \tag{6}$$

where S has been deformed to a new surface S' by applying an infinitesimal profile deformation, δS, in the local normal direction, $\vec{n}_S$, at a point, $\vec{x}$, on the surface, as shown above in Fig. 1.

Surface shape deformations will result in variations of the pressure distribution along the surface, so we will focus on pressure-based functionals with the form

$$j_S = \vec{d} \cdot (p\vec{n}_S). \tag{7}$$

The vector $\vec{d}$ is the force projection vector, and it is an arbitrary, constant vector which can be chosen to relate the pressure, p, at the surface to a desired quantity of interest. For aerodynamic applications, example candidates are

$$\begin{aligned}
&C_{\mathrm{D}}: && \vec{d} = \frac{1}{C_\infty}\left(\cos\alpha\cos\beta, \sin\alpha\cos\beta, \sin\beta\right), \\
&C_{\mathrm{L}}: && \vec{d} = \frac{1}{C_\infty}\left(-\sin\alpha, \cos\alpha, 0\right), \\
&C_{\mathrm{SF}}: && \vec{d} = \frac{1}{C_\infty}\left(-\sin\beta, \cos\alpha, -\sin\beta\sin\alpha, \cos\beta\right), \\
&C_{\mathrm{L}}/C_{\mathrm{D}}: && \vec{d} = \frac{1}{C_\infty C_D}\left(-\sin\alpha - \frac{C_L}{C_D}\cos\alpha\cos\beta, -\frac{C_L}{C_D}\sin\beta, \cos\alpha - \frac{C_L}{C_D}\sin\alpha\cos\beta\right),
\end{aligned} \tag{8}$$

where $C_\infty = \rho_\infty V_\infty^2 A / 2$, V_∞ is the freestream velocity, ρ_∞ is the freestream density, and A is a reference area.

The minimization of Eqn. (5) can be considered a problem of optimal control whereby the behavior of the governing flow equation system is controlled by the surface shape with deformations of the surface acting as the control input. Furthermore, any variations of the flow variables due to surface deformations are constrained to satisfy the system of governing flow equations,

$$R(U) = \frac{\partial U}{\partial t} + \nabla \cdot \vec{F}_{mov} = \frac{\partial U}{\partial t} + \nabla \cdot \vec{F} - \nabla \cdot (U \otimes \vec{u}_b) = 0, \tag{9}$$

where the terms involving the control volume motion have been separated from the traditional Euler fluxes. Mathematically, the constrained optimization problem can be formulated as follows:

$$\begin{aligned} &\text{Minimize} \quad J = \frac{1}{T}\int_{t_0}^{t_f}\int_{S} \vec{d}\cdot(p\vec{n}_S)dsdt \\ &\text{Such that} \quad R(U) = 0 \end{aligned} \tag{10}$$

Following the adjoint approach to optimal design, the constrained optimization problem in Eqn. (10) can be transformed into an unconstrained optimization problem by adding the inner product of an unsteady adjoint variable vector, ψ, and the governing equations integrated over the domain (space and time) to form the Lagrangian:

$$J = \frac{1}{T}\int_{t_0}^{t_f}\int_{S} \vec{d}\cdot(p\vec{n}_S)dsdt + \frac{1}{T}\int_{t_0}^{t_f}\int_{\Omega} \Psi^T R(U)d\Omega dt, \tag{11}$$

where we have introduced the adjoint variables, which operate as Lagrange multipliers and are defined as

$$\Psi = \begin{Bmatrix} \psi_\rho \\ \psi_{\rho u} \\ \psi_{\rho v} \\ \psi_{\rho w} \\ \psi_{\rho E} \end{Bmatrix} = \begin{Bmatrix} \psi_\rho \\ \vec{\varphi} \\ \psi_\rho \end{Bmatrix}. \tag{12}$$

To find the gradient information needed to minimize the objective function, we take the first variation of Eqn. (11) with respect to perturbations of the surface shape:

$$\delta J = \frac{1}{T}\int_{t_0}^{t_f}\int_{S} (\vec{d}\cdot\nabla p)\delta S dsdt + \frac{1}{T}\int_{t_0}^{t_f}\int_{S} (\vec{d}\cdot\vec{n}_S)\delta p dsdt + \frac{1}{T}\int_{t_0}^{t_f}\int_{\Omega} \Psi^T \delta R(U)d\Omega dt. \tag{13}$$

It is important to note that the first two terms of Eqn. (13) are found by using a result from previous work by Palacios, et. al.[1] based on differential geometry formulas, and this is a key feature differentiating the current formulation from other adjoint approaches. The third term of Eqn. (13) can be expanded by including the linearized version of the governing equations with respect to small perturbations of the design surface,

$$\begin{aligned} \delta R(U) &= \frac{\partial}{\partial t}(\delta U) + \nabla\cdot\delta\vec{F} - \nabla\cdot\delta(U\otimes\vec{u}_b) \\ &= \frac{\partial}{\partial t}(\delta U) + \nabla\cdot\left(\frac{\partial\vec{F}}{\partial U}\delta U\right) - \nabla\cdot\left[\frac{\partial(U\otimes\vec{u}_b)}{\partial U}\delta U\right] \\ &= \frac{\partial}{\partial t}(\delta U) + \nabla\cdot\left(\vec{A} - \bar{\bar{I}}\vec{u}_b\right)\delta U, \end{aligned} \tag{14}$$

along with the linearized form of the boundary condition at the surface,

$$\delta\vec{v}\cdot\vec{n}_S = -(\vec{v}-\vec{u}_b)\cdot\delta\vec{n}_S - \partial_n(\vec{v}-\vec{u}_b)\cdot\vec{n}_S\delta S \tag{15}$$

where $\vec{A}$ is the Jacobian of $\vec{F}$ using conservative variables. Eqn. (14) can now be introduced into Eqn. (13) to produce

$$\delta J = \frac{1}{T}\int_{t_0}^{t_f}\int_{S} (\vec{d}\cdot\nabla p)\delta S dsdt + \frac{1}{T}\int_{t_0}^{t_f}\int_{S} (\vec{d}\cdot\vec{n}_S)\delta p dsdt + \frac{1}{T}\int_{t_0}^{t_f}\int_{\Omega} \Psi^T\frac{\partial}{\partial t}(\delta U)d\Omega dt + \frac{1}{T}\int_{t_0}^{t_f}\int_{\Omega} \Psi^T\nabla\cdot(\vec{A}-\bar{\bar{I}}\vec{u}_b)\delta U d\Omega dt \tag{16}$$

By removing any dependence on variations of the flow variables, δp, the variation of the objective function for multiple surface deformations can be found *without* the need for multiple flow solutions which results in a

computationally efficient method for aerodynamic design involving many design variables. We now perform manipulations to remove this dependence. After changing the order of integration, integrating the third term of Eqn. (16) by parts gives

$$\int_{t_0}^{t_f}\int_{\Omega}\Psi^T\frac{\partial}{\partial t}(\delta U)d\Omega dt=\int_{\Omega}\left[\Psi^T\delta U\right]_{t_0}^{t_f}d\Omega-\int_{t_0}^{t_f}\int_{\Omega}\frac{\partial\Psi^T}{\partial t}\delta U d\Omega dt \tag{17}$$

A zero-value initial condition for the adjoint variables can be imposed, and assuming an unsteady flow with periodic behavior, the first term on the right hand side of Eqn. (17) can be eliminated with the following temporal conditions (the cost function does not depend on t_f):

$$\Psi(\vec{x},t_0)=0, \tag{18}$$

$$\Psi(\vec{x},t_f)=0. \tag{19}$$

Now, integrating the fourth term of Eqn. (16) yields

$$\int_{t_0}^{t_f}\int_{\Omega}\Psi^T\nabla\cdot(\vec{A}-\bar{\bar{I}}\vec{u}_b)\delta U d\Omega dt=\int_{t_0}^{t_f}\int_{\Omega}\nabla\cdot\left[\Psi^T(\vec{A}-\bar{\bar{I}}\vec{u}_b)\delta U\right]d\Omega dt-\int_{t_0}^{t_f}\int_{\Omega}\nabla\Psi^T(\vec{A}-\bar{\bar{I}}\vec{u}_b)\delta U d\Omega dt, \tag{20}$$

and applying the divergence theorem to the first term on the right hand side of Eqn. (20), assuming a smooth solution, gives

$$\begin{aligned}\int_{t_0}^{t_f}\int_{\Omega}\Psi^T\nabla\cdot(\vec{A}-\bar{\bar{I}}\vec{u}_b)\delta U d\Omega dt=&\int_{t_0}^{t_f}\int_{S}\Psi^T(\vec{A}-\bar{\bar{I}}\vec{u}_r)\cdot\vec{n}_S\delta U ds dt\\&+\int_{t_0}^{t_f}\int_{\Gamma_\infty}\Psi^T(\vec{A}-\bar{\bar{I}}\vec{u}_r)\cdot\vec{n}_S\delta U ds dt\\&-\int_{t_0}^{t_f}\int_{\Omega}\Psi^T(\vec{A}-\bar{\bar{I}}\vec{u}_b)\cdot\vec{n}_S\delta U d\Omega dt.\end{aligned} \tag{21}$$

With the appropriate choice of characteristic-based boundary conditions, the integral over the far-field boundary can be forced to vanish. Combining and rearranging the results from Eqns. (16), (17), (18), (19), and (21) yields an intermediate expression for the variation of the cost function,

$$\begin{aligned}\delta J=&\frac{1}{T}\int_{t_0}^{t_f}\int_{S}(\vec{d}\cdot\nabla p)\delta S ds dt+\frac{1}{T}\int_{t_0}^{t_f}\int_{S}(\vec{d}\cdot\vec{n}_S)\delta p ds dt+\frac{1}{T}\int_{t_0}^{t_f}\int_{S}\Psi^T(\vec{A}-\bar{\bar{I}}\vec{u}_b)\cdot\vec{n}_S\delta U ds\\&-\frac{1}{T}\int_{t_0}^{t_f}\int_{\Omega}\left[\frac{\partial\Psi^T}{\partial t}+\nabla\Psi^T\cdot(\vec{A}-\bar{\bar{I}}\vec{u}_b)\right]\delta U d\Omega dt.\end{aligned} \tag{22}$$

The final term of Eqn. (22) can also be made to vanish, if its integrand is zero at every point in the domain. When set equal to zero, the terms within the brackets constitute the set of partial differential equations which are commonly referred to as the adjoint equations. Therefore, the domain integral will vanish provided that the adjoint equations are satisfied as

$$\frac{\partial\Psi^T}{\partial t}+\nabla\Psi^T\cdot(\vec{A}-\bar{\bar{I}}\vec{u}_b)=0\quad\text{in }\Omega, \tag{23}$$

or, after taking the transpose,

$$\frac{\partial \Psi}{\partial t} + (\vec{A} - \bar{\bar{I}}\vec{u}_b) \cdot \nabla \Psi = 0 \text{ in } \Omega. \tag{24}$$

The accompanying boundary condition will be given below. Furthermore, the surface integral in the third term on the right hand side of Eq. (22) can be evaluated given our knowledge of $\vec{A}$, $\vec{u}_b$, the wall boundary condition, $(\vec{v} - \vec{u}_b) \cdot \vec{n}_S = 0$, and the linearized wall boundary condition in Eq. (15). By leveraging previous derivation of Economon, Palacios, et. al[10] with some slight modifications and including time integration, it can be shown that evaluating the surface integral and rearranging the variation of the functional gives

$$\delta J = \frac{1}{T}\int_{t_0}^{t_f}\int_S \left[(\vec{d} \cdot \nabla p) + (\nabla \cdot \vec{v})\upsilon + (\vec{v} - \vec{u}_b) \cdot \nabla(\upsilon) \right] \delta S ds dt + \frac{1}{T}\int_{t_0}^{t_f}\int_S \left[\vec{d} \cdot \vec{n}_S - \vec{n}_S \cdot \vec{\varphi} - \psi_{\rho E}(\vec{v} \cdot \vec{n}_S) \right] \delta p ds dt, \tag{25}$$

where $\upsilon = \rho\psi_\rho + \rho\vec{v} \cdot \vec{\varphi} + \rho H \psi_{\rho E}$. Therefore, the adjoint equations with the admissible adjoint boundary condition that eliminates the dependence on the fluid flow variations (δp) by forcing the second term on the right hand side of Eq. (25) to vanish can be written as

$$\begin{aligned} &\frac{\partial \Psi}{\partial t} + (\vec{A} - \bar{\bar{I}}\vec{u}_b)^T \cdot \nabla \Psi = 0 \quad \text{in } \Omega, \\ &\vec{n}_S \cdot \vec{\varphi} = \vec{d} \cdot \vec{n}_S - \psi_{\rho E}(\vec{v} \cdot \vec{n}_S) \quad \text{on S}, \end{aligned} \tag{26}$$

and the variation of the objective function becomes

$$\delta J = \frac{1}{T}\int_{t_0}^{t_f}\int_S \left[(\vec{d} \cdot \nabla p) + (\nabla \cdot \vec{v})\upsilon + (\vec{v} - \vec{u}_b) \cdot \nabla(\upsilon) \right] \delta S ds dt = \frac{1}{T}\int_{t_0}^{t_f}\int_S \frac{\partial J}{\partial S} \delta S ds, \tag{27}$$

where

$$\frac{\partial J}{\partial S} = \vec{d} \cdot \nabla p + (\nabla \cdot \vec{v})\upsilon + (\vec{v} - \vec{u}_b) \cdot \nabla(\upsilon) \tag{28}$$

is what we call the *surface sensitivity*. The surface sensitivity provides a measure of the variation of the objective function with respect to infinitesimal variations of the surface shape in the direction of the local surface normal. This value is computed at each surface node of the numerical grid at each physical time step with negligible computational cost. Note that the final expression for the variation involves only a surface integral at each physical time step and has no dependence on the volume mesh.

C. Adjoint Application to Local Blade Aerodynamics

The three-dimensional adjoint sensitivities can be used to approximate the two-dimensional aerodynamics at each airfoil station required for CSD analysis. First, C_Q and C_T are expressed as integrations over the blade length

$$C_Q = \frac{Q}{\rho_\infty A_D V_t^2 R} = \frac{1}{\rho_\infty A_D V_t^2 R}\int_0^R r d(r) dr \tag{29}$$

$$C_T = \frac{F_T}{\rho_\infty A_D V_t^2} = \frac{1}{\rho_\infty A_D V_t^2}\int_0^R l(r) dr, \tag{30}$$

where $d(r)$ and $l(r)$ are the radial distributions of drag and lift per unit length. For the purposes of this discussion, d is in the plane perpendicular to the axis of rotation and l is parallel to the axis of rotation. The total incident velocity includes the rotor axis tilt and the blades' mechanical motions (control and structural deformations). These can be expressed in terms of the local (two-dimensional) drag and lift coefficients though Eqs. (31) and (32):

$$d = \frac{\partial D}{\partial r} = \frac{c}{2}\rho_\infty a_\infty^2 M(r)^2 c_d \tag{31}$$

$$l = \frac{\partial L}{\partial r} = \frac{c}{2}\rho_\infty a_\infty^2 M(r)^2 c_l \tag{32}$$

Combining Eqns. (31,32) with Eqs. (29,30) and differentiating both sides with respect to r, c_d and c_l can be expressed as radial gradients of C_Q and C_T as

$$c_d(r) = \frac{2\pi\omega^2 R^5}{c a_\infty^2 r M(r)^2}\left.\frac{\partial C_Q}{\partial r}\right|_r \tag{33}$$

$$c_l(r) = \frac{2\pi\omega^2 R^4}{c a_\infty^2 M(r)^2}\left.\frac{\partial C_F}{\partial r}\right|_r . \tag{34}$$

The adjoint solution, discussed above, will yield the gradient of C_Q and C_T with respect to normal displacement of any given node on the surface of the blade. Along any airfoil section, which is always perpendicular to the blade axis, the surface-normal direction ($\vec{n}$) will always be orthogonal to the radial direction. Differentiating Eqns. (33) and (34) with respect to the local normal direction and rearranging, the adjoint sensitivity of c_d and c_l are given by

$$\left.\frac{\partial c_d}{\partial n}\right|_r = \left[\frac{2\pi\omega^2 R^5}{c a_\infty^2 M(r)^2}\right]\frac{1}{r}\frac{\partial}{\partial r}\left.\left(\frac{\partial C_Q}{\partial n}\right)\right|_r \tag{35}$$

$$\left.\frac{\partial c_l}{\partial n}\right|_r = \left[\frac{2\pi\omega^2 R^4}{c a_\infty^2 M(r)^2}\right]\frac{\partial}{\partial r}\left.\left(\frac{\partial C_T}{\partial n}\right)\right|_r . \tag{36}$$

Hence, the sensitivity of the two-dimensional (airfoil) aerodynamics to nodal motion in the surface-normal direction by be found directly from already-computed adjoint sensitivities to C_Q and C_T provided the normal and radial direction are kept orthogonal on the blade's surface mesh. It is noted that the moment coefficient, C_m (the airfoil moment about the beam axis), was also required by the CSD tool. The procedure discussed above does not address this since no adjoint surfaces are available from which Cm can be expressed. This is addressed in the discussion of future directions below.

III. Problem Formulation & Global Optimization Architecture

Rotorcraft optimization procedure generally involves loose coupling, or exchanging data between multiple disciplines iteratively until a multidisciplinary convergence is reached for a given design. The primary necessity of this process in rotorcraft applications is the motion of the rotor blades as they revolve. In addition to revolution (which changes the incident flow conditions of the blade in forward flight), each blade experiences a number of cyclic control motions and structural deformations that are large compared to the geometry of the blade. All of these motions have significant effects on the aerodynamic loading on blades yielding the need for coupling the control of the blades, their structural deformations, and their aerodynamic loading in some fashion. Tight coupling involves solving both the fluid and structural simultaneously at each step of a time-accurate solution. A generalized soft coupling procedure is shown in Fig. 2 below. The aerodynamic properties of interest (in this case CQ and CT) and their sensitivities (if applicable) are typically averaged over all time instances of a periodically-steady revolution.

The soft coupling procedure outlined above is effective but costly. Each design point requires an inner loop iteration with multiple evaluations of both the CFD tool (typically the vast majority of the total expense) and a CSD tool. In this study, adjoint surface sensitivities were used to modify the procedure and eliminate the inner loop. Instead of exchanging only aerodynamic loading data with the CSD tool, surface sensitivities were exchanged which provide a local, linear approximation of aerodynamic loading changes with changes in shape in addition to providing gradient information to the global optimizer. Hence, an optimization procedure was performed with only: a) the CSD tool and b) a linearized model of aerodynamic performance in place of the CFD tool. This new inner loop produces an approximate optimum which is then evaluated with a new CFD and corresponding adjoint solutions in the outer loop. While the computation of the adjoint sensitivities adds expense, the total number of CFD solutions required is decreased. In addition, the procedure can be run in an asynchronous fashion, with iterative improvements being made when CFD resources are available.

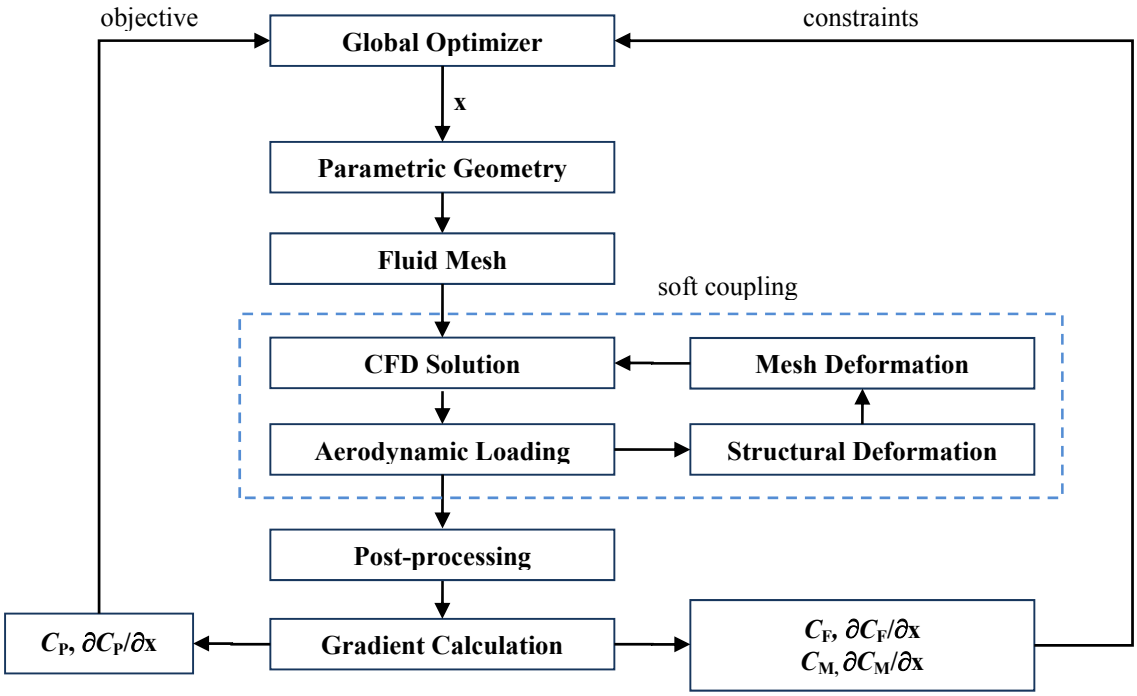

Figure 2. Schematic representation of a generalized soft coupling global optimization process. CFD and CSD tools exchange data in the inner loop with design modification driven by the global optimizer (outer loop). Note that power coefficient (C_P) has been assumed as the objective while generic force and moment coefficients are assumed as constraints, but any quantity of interest could be used for either. Gradient evaluation method is arbitrary.

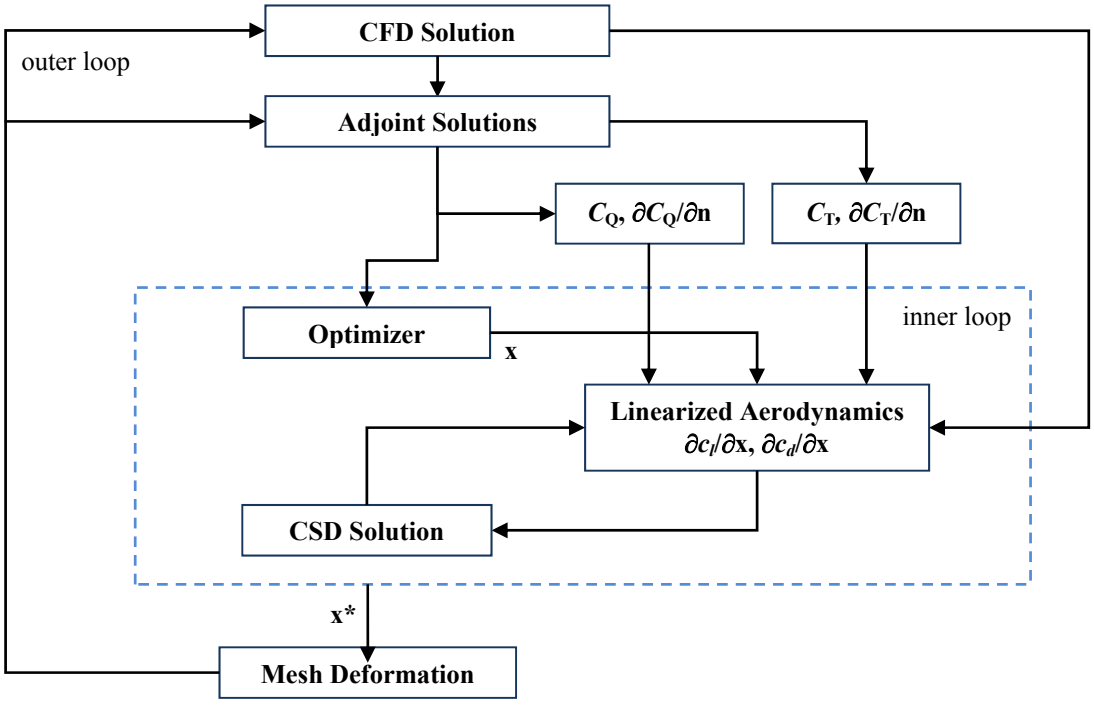

Figure 3. Schematic representation of modified global optimization process used presently. A single set of CFD and adjoint solutions are used to develop a linear model for the inner loop. The inner loop iterates to an optimum solution with low-cost tools before providing a new design to the mesh deformation, CFD, and adjoint solutions (high-cost tools). This procedure eliminates the need for inner-loop soft coupling and the evaluation of a number of CFD solutions per design evaluation.

This new procedure, viewed from the outer loop, in analogous to a sequential linear programming (SLP) approach to the aerodynamic inputs of the CSD tool. The CFD tool is still used with prescribed deformations from the coupled CSD-linearized aerodynamics optimum and is therefore still a form of loose coupling. In addition, no provision was made in this study for modifications to the structural properties of the blades due to deformations of their shape. This, however, was due only to a lack of data concerning the internal structure of the blades studied and is not limited by the MDO architecture itself. With structural details of the blades, the appropriate structural stiffnesses and other properties required by the CSD tool would simply be updated in the inner loop. The modified procedure used in this study is shown above in Fig. 3.

Since the inner loop no longer requires expensive function evaluations, both a large number of design variables and an arbitrary optimization algorithm can be used. This interacts in a convenient way with the adjoint surface sensitivities and free form deformation (FFD) geometric modification scheme used in this study since arbitrarily fine control of the geometry is possible via surface sensitivities produced from a single adjoint calculation. The linearized aerodynamic model, however limits the size of the changes possible in the inner optimization loop to a small range in which the approximation is valid.

While the linearized aerodynamic model replaces the need for need for CFD evaluations in the inner loop, the aerodynamic loading on the blades still needs to be adjusted to correspond to changes in the blade deformations. This was done via the linearized aerodynamic model and the FFD control points. The CSD tool predicts the displacements of airfoil sections parallel and perpendicular to the axis of rotation in addition to the local rotation about the beam axis. These deformations were mapped to the FFD control points and interpolated before computing the changes in aerodynamic loading due to changes in blade deformations. This completes the inner loop of Fig. 3.

IV. Rotor Model

A single UH-60A rotor blade was modeled in inviscid flow. The optimization architecture outlined above does not place any limits on the fidelity of the CFD simulation; this model was chosen as a convenient demonstration to to save computational cost. A multiple blade (full rotor) model is preferable to include wake interactions between the blades. To minimize these inaccuracies, a high-speed forward flight case (C8534) was chosen. The blade surface mesh and free-form deformation box are shown below in Fig. 4. The solid blade geometry was constructed from a sequence of airfoil sections with a portion inward of the innermost section (highlighted in Fig. 4) added to prevent unrealistic and disruptive vortex shedding on the blade's inner edge. (No geometry inward of the innermost airfoil section was available for this study.) The FFD box surrounded the blade to encompass everything except for the added section inward of the root airfoil section. Topological dimensions of eight cells (radial) by eight cells (chord-wise) by one cell (vertical) were chosen. The face of nodes corresponding to the innermost airfoil section was held fixed to prevent unrealistic or unsmooth deformations. The radial position of the nodes were held fixed with blade thickness and chord directions free, resulting in a total of 288 design variables. An upper limit on FFD control point motion of 1% root chord was found to yield acceptable results through trial and error.

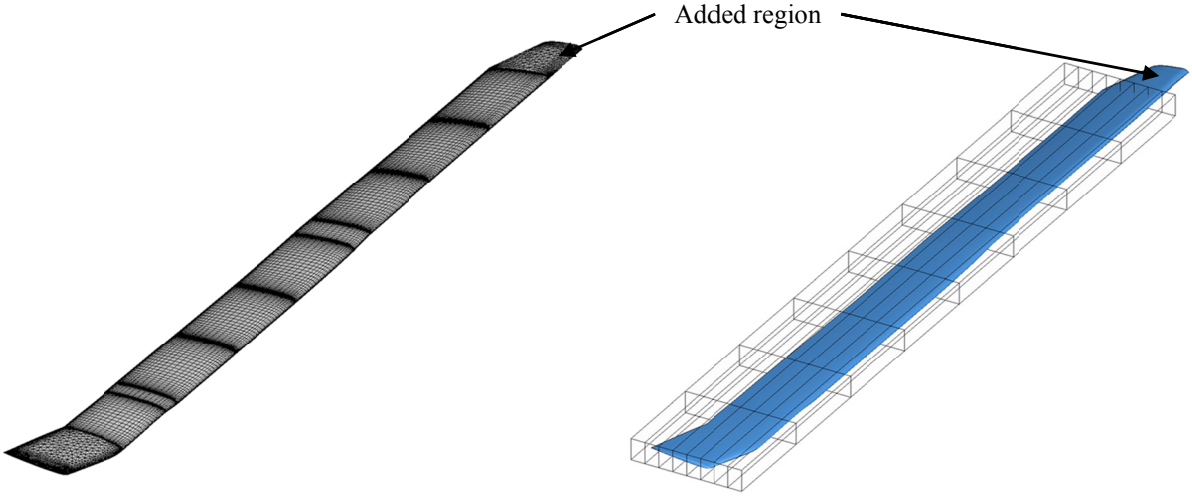

Figure 4. Surface mesh (left) and FFD geometry parameterization (right) of single UH-60A rotor blade.

Mesh deformations (displacements and rotations of the airfoil sections along the blade) from UMARC we mapped to the three-dimensional surface mesh at each time (azimuth) step. A step size of 2.5° was chosen to correspond exactly with the spacing used in UMARC (preventing the need for interpolation) which provided sufficient stability in the CFD solution. (The explicit mesh motion included in the CFD solutions required fairly conservative solver numerical settings). Three full revolutions were taken to overcome any initialization effects and achieve a periodic steady state. Three revolutions of the adjoint solutions for C_Q and C_T was also used (beginning with the last flow solution step). Of these solutions, the middle revolution was isolated and used to compute time-averaged sensitivities.

V. Results

This section describes the result from an outer iteration loop. The time histories of C_Q and C_T are shown below in Fig. 5. As expected for this flight case, periodic flow emerged rapidly with the second and third revolutions of the flow solution nearly exactly equal.

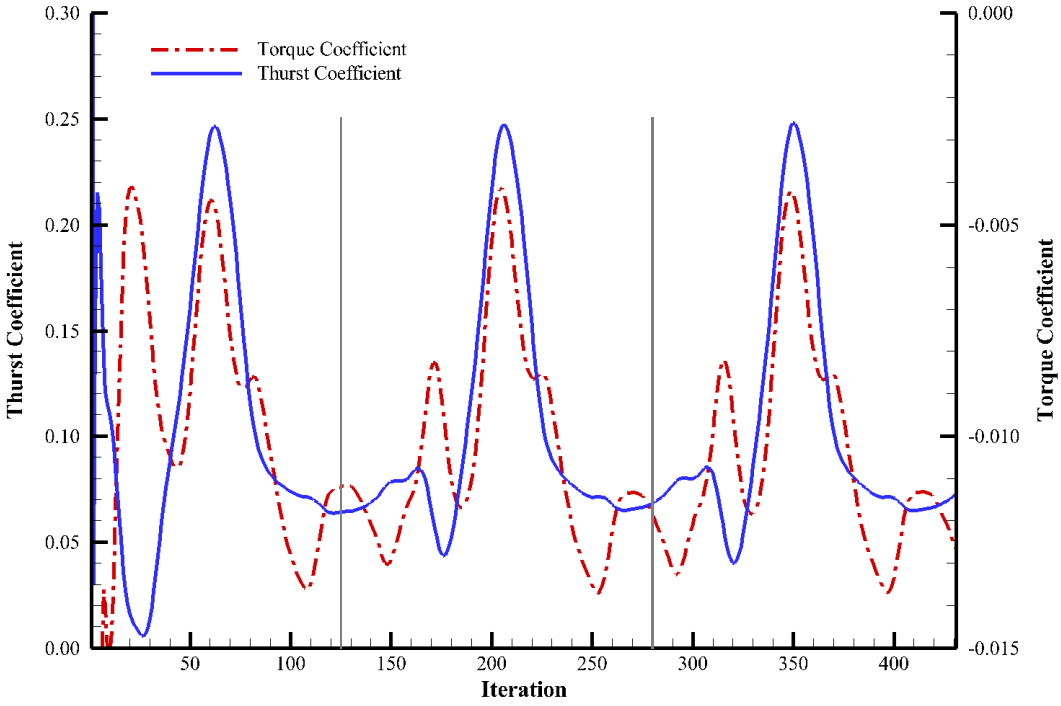

Figure 5. Time histories of C_Q and C_T for three revolutions of a flow solution.

Inner loop optimization was carried out to minimize C_Q without reducing C_T from its nominal (original) value. The resulting deformations modified the blade tip most heavily as expected. Contours of the flow and adjoint solutions for a full revolution are shown in Figs. 6, corresponding flow and adjoint surface sensitivity contours for a specific time step are shown in Fig. 7, and the deformed blade and FFD box are shown in Fig. 8. After one full outer loop (baseline CSD solution, CFD and adjoint solutions, inner loop optimization, and final CSD solution to trim), C_Q was reduced by 7.07% with no numerically significant change in C_T.

The authors emphasize that these results are preliminary and the focus of this study was the method and not the result above. In order to improve and verify the results, more high-fidelity (CFD with coupled mesh motion) iterations are required until the outer loop reaches a convergence (sufficiently small design changes between subsequent $\mathbf{x}^*$). In addition, a full rotor, viscous model is required to capture all the relevant flow interactions. Subsequent CFD analysis was beyond the computational scope of this work but will be investigated in the future. However, within the bounds of a linearized aerodynamic model based on adjoint sensitivities and a small bounding box on changes in the design variables, significant improvement was shown in a single outer loop.

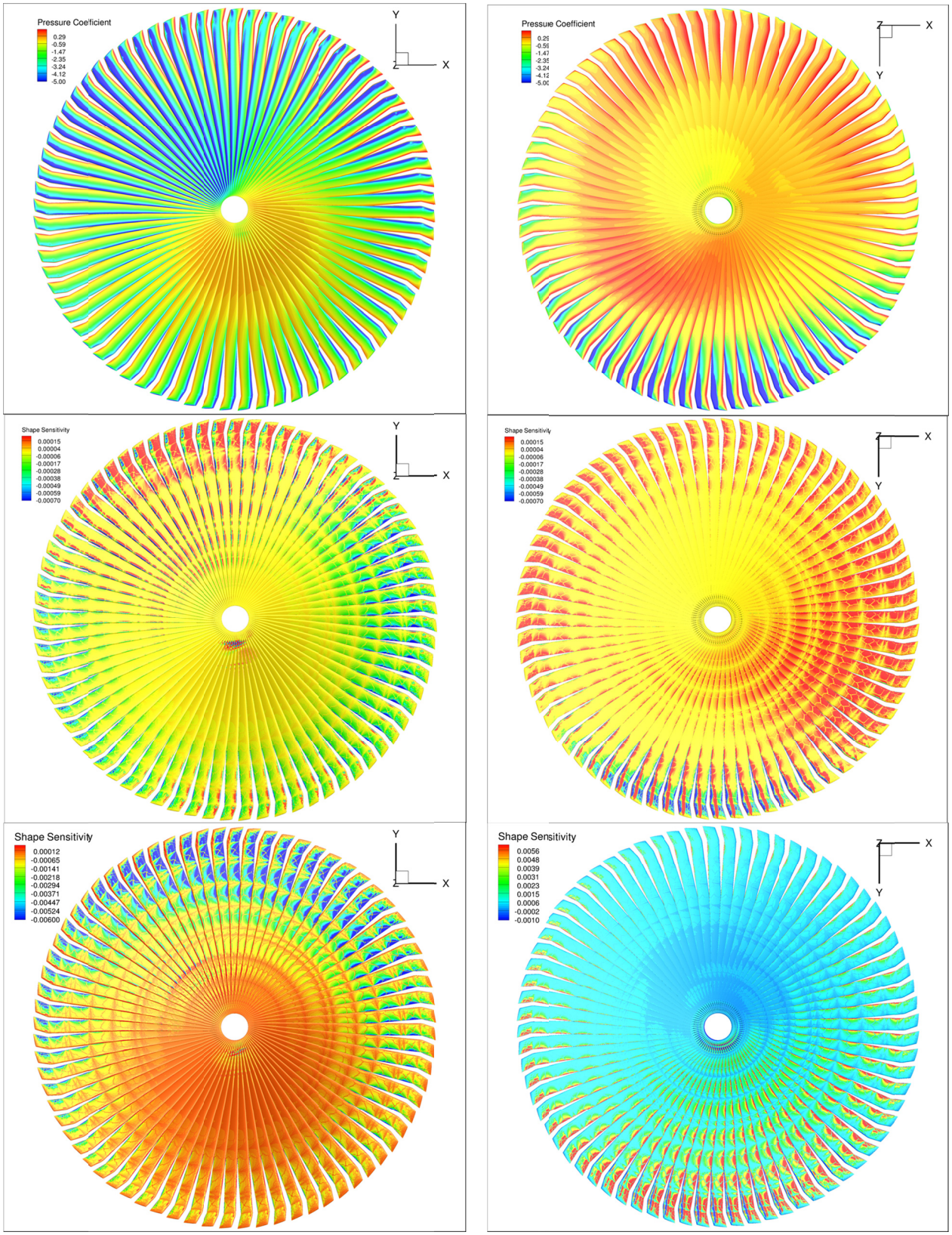

Figure 6. Contours over a full revolution: upper surface C_p (top left), C_p lower surface (top right), C_Q sensitivity upper surface, (middle left), C_Q sensitivity lower surface (middle right), C_T sensitivity upper surface, (bottom left), C_T sensitivity lower surface (bottom right) Free stream flow is along positive x at $\alpha = 0$.

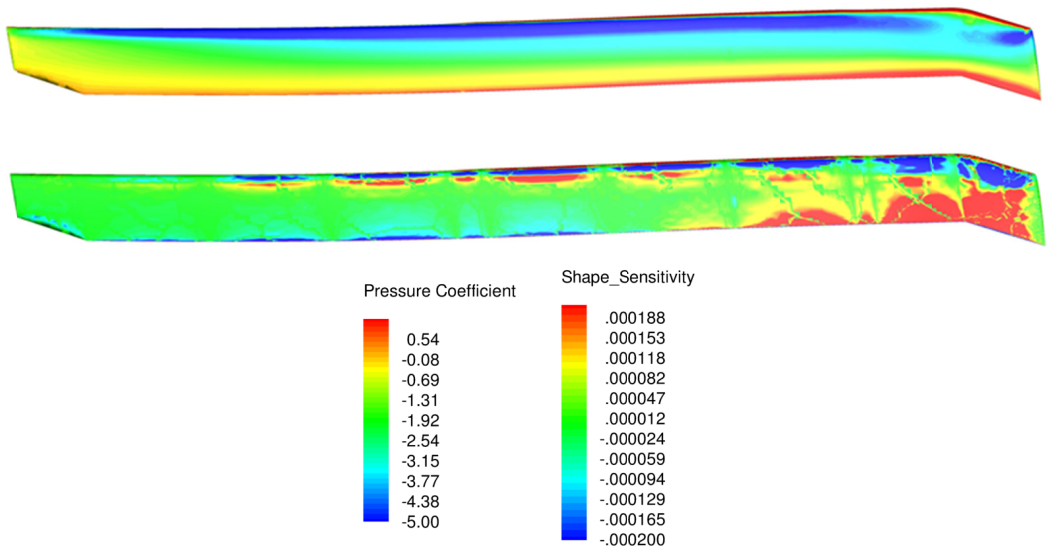

Figure 7. Corresponding C_p (top) and surface sensitivity (bottom) contours corresponding to $\phi = 90°$.

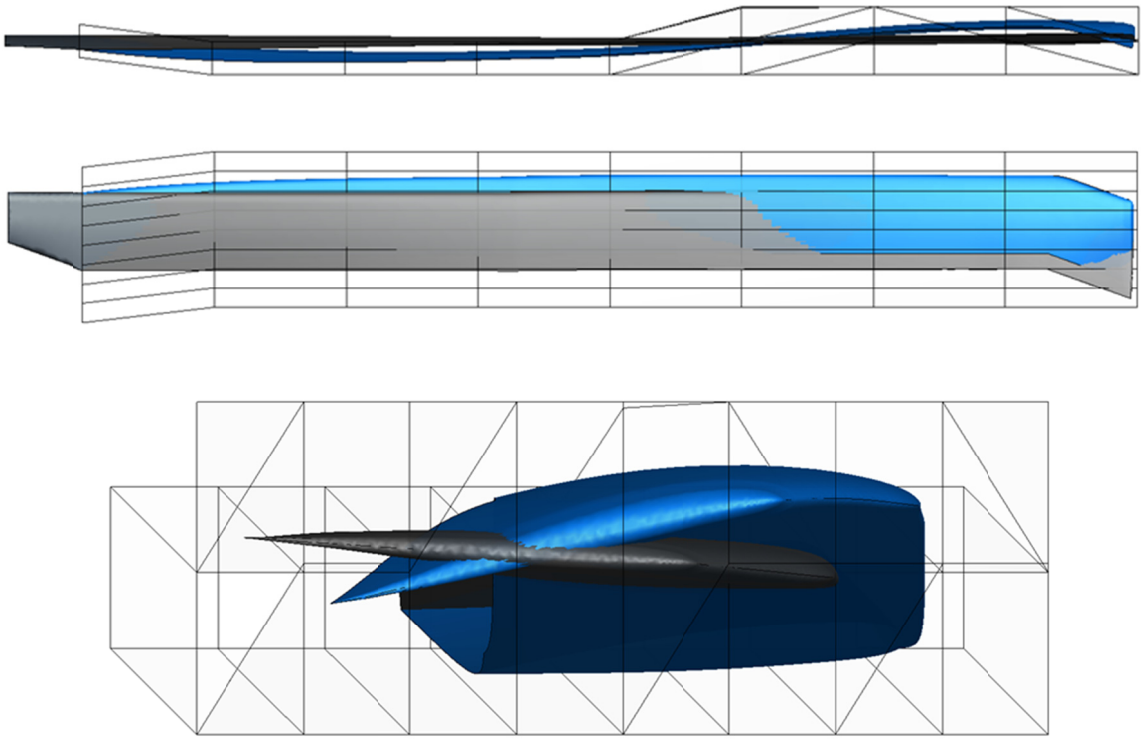

Figure 8. Deformed blade (blue) compared to original blade (grey) and FFD box after inner loop optimization with twenty-fold amplification for visualization. Note the uniform forward sweep at every control point, the "S"-shaped deformation in the radial direction, and the added positive twist towards the blade tip.

VI. Future Directions

Numerous future directions exist for this work. Near-term improvements to the results presented here require only a larger computational budget while longer-term items require additional tool development within the SU^2 framework. Near-term items include:

1. The use of full rotor models with viscous flow physics
2. Bringing the process described above to convergence with an adequate number of outer loops
3. Increased number of design variables in the FFD formulation

Additional functionality will improve both the efficiency and fidelity of the simulations and optimization framework, including:

1. Implementing a time-spectral solver in SU2 consistent with previous studies
2. Accounting for modification of the structural stiffness of the blade sections under deformation
3. Addition of fixed-wing functionals (C_L, C_D, and C_M) to rotating frames enabling c_l, c_d, and c_m sensitivities to be computed directly.

Together, these changes enable a more efficient and higher-fidelity rotorcraft optimization framework.

Acknowledgments

This work has been carried out under the support of the Aerofightdynamics Directorate (AFDD) at NASA Ames Research Center. We acknowledge their support in the forms of both technical data and the advice. In addition the authors would like to thank Anubhav Datta for answering our innumerable questions and the University of Maryland (and Asitav Mishra) for support of UMARC. Thomas Economon and Francisco Palacios of Stanford University are acknowledged for their unwavering support and constant development of SU^2 which made this study possible.

References

[1] Bueno-Orovio, A., Castro, C., Palacios, F., and Zuazua, E., "Continuous Adjoint Approach for the Spalart-Allmaras Model in Aerodynamic Optimization", *AIAA Journal*, Vol. 50, No. 3, pp. 631-646, March 2012.
[2] Caradonna, F. X. and Tung, C., "Experimental and Analytical Studies of a Helicopter Rotor in Hover", NASA Technical Memorandum 81232, September 1981.
[3]Choi, S., Alonso, J. J., Van der Weide, E., and Sitaraman, J., "Validation Study of Aerodynamic Analysis Tools for Design Optimization of Helicopter Rotors", AIAA Paper 07-3929, Miami FL, June 2007.
[4]Choi, S., and Datta, A., "Time-Spectral Method for the CFD Prediction of Main Rotor Vibratory Loads," *5th International Conference on CFD*, Seoul, Korea, July 2008.
[5]Choi, S., Datta, A., and Alonso, J. J., "Prediction of Helicopter Rotor Loads Using Time-Spectral Computational Fluid Dynamics and an Exact Fluid–Structure Interface," *Journal of the American Helicopter Society*, Vol. 56, 042001, 2011.
[6]Choi, S., and Datta, A., "CFD Prediction of Rotor Loads using Time-Spectral Method and Exact Fluid-Structure Interface" *26th AIAA Applied Aerodynamics Conference*, Honolulu, HI, August 2008.
[7]Choi, S., Lee, K., Alonso, J. J., and Datta, A., "Study on Time-Spectral and Adjoint-Based Design Optimization of Helicopter Rotors," *AHS Specialist's Conference on Aeromechanics*, San Francisco, CA, Jan. 2008.
[8]Choi, S., Potsdam, M., Lee. K., Iaccarino, G, and Alonso, J.J., "Helicopter Rotor Design Using a Time-Spectral and Adjoint-Based Method", *12th AIAA/ISSMO Multidisciplinary Analysis and Optimization Conference*, Victoria, BC, Sept. 2008.
[9] Durmont, A., Le Pape, A., Peter, J., and Huberson, S., "Aerodynamic Shape Optimization of Hovering Rotors Using a Discrete Adjoint of the Reynolds-Averaged Navier–Stokes Equations", *Journal of the American Helicopter Society*, Vol. 56, 032002, 2011.
[10] Economon T. D., Palacios, F., Alonso, J. J., "Optimal Shape Design for Open Rotor Blades", *30th AIAA Applied Aerodynamics Conference*, New Orleans, LA, June, 2012.
[11] Economon, T. D., Palacios, F., Alonso, J. J., "Unsteady Aerodynamic Design on Unstructured Meshes with Sliding Interfaces and Active Flow Control," *51st AIAA Aerospace Sciences Meeting*, Grapevine, TX, Jan. 2013.
[12] Gopinath, A. K. and Jameson, A., "Time Spectral Method for Periodic Unsteady Computations over Two- and Three-Dimensional Bodies", *43th AIAA Aerospace Sciences Meeting*, Reno, NV, January 2005.
[13] Jameson, A., "Aerodynamic Design via Control Theory", *Journal of Scientific Computing*, 3:233-260, 1988.
[14] Jayaraman, B., Wissink, A.M., Joon W. Lim, J.W., Potsdam, M., and Dimanlig, A.C.B., "Helios Prediction of Blade-Vortex Interaction and Wake of the HART II Rotor", *50th AIAA Aerospace Sciences Meeting*, Nashville, TN, January 2012.
[15] Le Pape, A., and Beaumier, P., "Numerical Optimization of Helicopter Rotor Aerodynamic Performance in Hover", *Aerospace Science and Technology*, Vol. 9, Issue 3, pp. 191-20, April 2005.
[16]Leoviriyakit, K., and Jameson, A., "Aero-structural Wing Planform Optimization," *42nd Aerospace Science Meetings & Exhibit*, Reno, NV, Jan. 2004.
[17] Martins, J. R. R. A., "A Coupled-Adjoint Method for High-Fidelity Aero-Structural Optimization", Ph.D Dissertation, Department of Aeronautics and Astronautics, Stanford University, Stanford, CA, Oct. 2002.

[18] McMullen, M. S., and Jameson, A., "The Computational Efficiency of Non-Linear Frequency Domain Methods," *Journal of Computational Physics*, Vol. 212, Issue 2, pp.637-661, March 2006.
[19] Nadarajah, S., McMullen, M., and Jameson, A., "Aeroelastic Solutions using the Time Accurate and Non-Linear Frequency Domain Methods", AIAA Paper 2006-0445, *44th Aerospace Sciences Meeting and Exhibit*, January 9 - 12, 2006, Reno, Nevada.
[20] Palacios, F., Alonso, J. J., Duraisamy, K., Colonno, M., Hicken, J., Aranake, A., Campos, A., Copeland, S., Economon, T. D., Lonkar, A., Lukaczyk, T., Taylor, T., "Stanford University Unstructured (SU^2): An Open Source Integrated Computational Environment for Multiphysics Simulation and Design," *51st AIAA Aerospace Sciences Meeting*, Grapevine, TX, Jan. 2013.
[21] Reuther, J. J., Jameson, A., Alonso, J. J., Rimlinger, M., and Saunders, D., "Constrained Multipoint Aerodynamic Shape Optimization Using an Adjoint Formulation and Parallel Computers: Part I & II", *Journal of Aircraft*, 36(1):51-74, 1999.
[22] Schmitz, S., Bhagwat, M., Moulton, M.A., Caradonna, F.X., Chattot, J., "The Prediction and Validation of Hover Performance and Detailed Blade Loads", *Journal of the American Helicopter Society*, Vol. 54, 032004, 2009.
[23] Stanford University Aerospace Design Laboratory (adl.stanford.edu).
[24] Stanford University Unstructured (SU^2): http://su2.stanford.edu.
[25] Tarzanin, F., and Young, D., "Boeing Rotorcraft Experience with Rotor Design and Optimization," AIAA-1998-4733, AIAA/USAF/NASA/ISSMO *7th Symposium on Multidisciplinary Analysis and Optimization*, St. Louis, MO, Sep. 2-4, 1998.
[26] University of Maryland.